Sequential Charge Separation in Two Axially Linked Phenothiazine–Aluminum(III) Porphyrin–Fullerene Triads

ARTICLE *in* THE JOURNAL OF PHYSICAL CHEMISTRY A · FEBRUARY 2011

Impact Factor: 2.69 · DOI: 10.1021/jp110156w · Source: PubMed

6 AUTHORS, INCLUDING:

Prashanth Poddutoori
University of Prince Edward Island
23 PUBLICATIONS **197** CITATIONS
SEE PROFILE

Atula S. D. Sandanayaka
Kyushu University
96 PUBLICATIONS **2,405** CITATIONS
SEE PROFILE

Osamu Ito
Tohoku University
591 PUBLICATIONS **15,887** CITATIONS
SEE PROFILE

THE JOURNAL OF PHYSICAL CHEMISTRY A

ARTICLE

pubs.acs.org/JPCA

Sequential Charge Separation in Two Axially Linked Phenothiazine−Aluminum(III) Porphyrin−Fullerene Triads

Prashanth K. Poddutoori,[†] Atula S. D. Sandanayaka,[‡] Niloofar Zarrabi,[†] Taku Hasobe,[‡,§] Osamu Ito,*[,∥] and Art van der Est*[,†]

[†]Department of Chemistry, Brock University, 500 Glenridge Avenue, St. Catharines, Ontario, Canada L2S 3A1

[‡]School of Materials Science, Japan Advanced Institute of Science and Technology, 1-1 Asahidai, Nomi, 923-1292, Japan

[§]Department of Chemistry, Faculty of Science and Technology, Keio University, 3-14-1 Hiyoshi, Kohoku-ku, Yokohama, Kanagawa 223-8522, Japan and PRESTO, Japan Science and Technology Agency (JST), 4-1-8 Honcho, Kawaguchi, Saitama, 332-0012, Japan

[∥]Fullerene Group, NIMS, Tsukuba, Japan and CarbonPhotoScience Lab, Kita-Nakayama 1-6, Sendai, 981-3215, Japan

Supporting Information

ABSTRACT: New supramolecular triads (PTZpy→AlPor−C_{60}, TPTZpy→AlPor−C_{60}), containing aluminum(III) porphyrin (AlPor), fullerene (C_{60}), and phenothiazine (phenothiazine = PTZ, 2-methylthiophenothaizine = TPTZ) have been constructed. In these triads the fullerene and phenothiazine units are bound axially to opposite faces of the porphyrin plane via covalent and coordination bonds, respectively. The ground- and excited-state properties of the triads and reference dyads are studied using steady-state and time-resolved spectroscopic techniques. The time-resolved data show that photoexcitation results in charge separation from the excited singlet state of the porphyrin to the C_{60} unit, generating (Donor)py→AlPor$^{\bullet+}$−$C_{60}^{\bullet-}$, Donor = PTZ and TPTZ. A subsequent hole shift from the porphyrin to phenothiazine generates the charge-separated state (Donor)$^{\bullet+}$py→AlPor−$C_{60}^{\bullet-}$. The lifetime of the charge separation exhibits a modest increase from 39 ns in the absence of the donor to 100 ns in PTZpy→AlPor−C_{60} and 83 ns in TPTZpy→AlPor−C_{60}. These lifetimes are discussed in terms of the electronic coupling between phenothiazine, the porphyrin, and C_{60}.

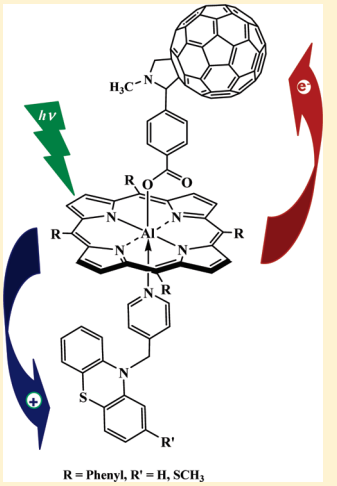

1. INTRODUCTION

Light-induced charge separation is the key step in the conversion of light energy into chemical energy in both natural and artificial photosynthesis. However, achieving efficient light-induced electron transfer in synthetic donor−acceptor (D−A) complexes remains a challenge despite the wide variety of complexes that have been prepared and studied.[1−8] The core of the problem is to find chemical structures that simultaneously optimize the parameters governing forward electron transfer while minimizing the rate of the back reaction. In designing such complexes, classical Marcus theory[9] provides a useful guide in understanding how the various properties should be varied, and it shows that the electron transfer rate depends on the free energy change and the reorganization energy of the reaction as well as the electronic coupling between the initial and final state electronic wave functions. The free energy changes of the possible electron transfer reactions in D−A complexes can be determined from the redox midpoint potentials of the donor(s) and acceptor(s) and from the excited-state energies of the chromophore, which are reflected in its absorption and emission properties. The reorganization energy depends on how the distribution of charge in the complex couples to the vibrational modes and on the polarity of the solvent. The electronic coupling is governed to a large extent by the nature of the bonding between the donor and acceptor.

To achieve a high quantum yield of light-induced charge separation with high energy conversion, the electron transfer should take place from the lowest excited singlet state of the chromophore and should be faster than other processes such as intersystem crossing. However, optimization of the rate of forward electron transfer from the excited singlet state generally also promotes charge recombination. Thus, secondary electron transfer is needed to stabilize the charge separation. One possibility is to attach a secondary donor that allows the electron hole created by the initial electron transfer to be shifted further away from the unpaired electron on the acceptor, thereby

Received: October 23, 2010
Revised: December 7, 2010
Published: December 29, 2010

increasing the lifetime of the charge separation.[10−17] A critical factor in determining how effectively the hole shift stabilizes the radical ion pair is the electronic coupling, which depends on the distance and the nature of the bonds between the electron transfer components (see refs 18 and 19 for reviews). Thus, it is of interest to investigate complexes with different bridging groups and geometries to determine how effectively they stabilize the charge separation.

Porphyrins are commonly used as the chromophore in D−A complexes,[2,6−8,13,20−25] due to their favorable redox and optical properties, which can be easily tuned by changing substitutions on the periphery and/or the element in the center of the porphyrin ring. Functionalized fullerene (C_{60}) has been shown to be an effective electron acceptor because the delocalization of the charge over the large three-dimensional fullerene moiety results a small reorganization energy,[12,22,24−31] which tends to increase the rate of charge separation (CS) and decrease the rate of charge recombination (CR).[26−31] Because of these favorable properties, porphyrin−fullerene systems have been widely prepared and studied.[12,32−36]

Recently, a number of donor−porphyrin−fullerene model compounds have been reported, which elegantly demonstrate that the lifetime of the final charge-separated state can be prolonged through secondary donation or cascade electron transfer.[37−41] In these complexes, the secondary donor and the fullerene are attached via a bridge containing σ- and/or π-bonds to the periphery of the porphyrin. Thus, the donor and acceptor lie in the same plane as the porphyrin ring, and the electron transfer takes place in this plane. Several systems in which the direction of the electron transfer is axial to the porphyrin plane have also been prepared.[42−48] An advantage of the axial arrangement is the placement of the donor and acceptor units on opposite faces of the porphyrin ensuring that they are spatially well separated and that unwanted nonbonded porphyrin−fullerene interactions[49] are minimized. Most of these axial systems show efficient electron transfer from the porphyrin to fullerene. However, stepwise or cascade electron transfer has not been studied in such complexes largely because of the difficulty associated with attaching two different axial ligands to the porphyrin.

Aluminum(III) porphyrins form axial covalent bonds with alcohols, carboxylic acids, and phosphinates; they have moderate redox potentials; and the high Lewis acidity of aluminum allows coordination by Lewis bases to form six-coordinate complexes.[50−54] Because of these unique properties, aluminum(III) porphyrin (AlPor) is a good candidate for constructing triads in which the electron acceptor and secondary donor are axial to the porphyrin ring. Recently, we reported the synthesis and photochemistry of a molecular triad in which fullerene was attached axially to AlPor and ferrocene was bound to the meso position of the porphyrin ring via a bridge that caused it to reside on the opposite face of the porphyrin from the fullerene.[48] Multistep electron transfer occurs in a direction largely perpendicular to the porphyrin ring in this system; however, a portion of the bridge is still in the porphyrin plane, and it is difficult to ensure that the secondary donor actually resides opposite to the fullerene unit since several conformers are possible.

Here, we report two new AlPor-based triads that avoid these problems by taking advantage of the ability of Al(III) to coordinate a second axial ligand such as pyridine to attach a secondary electron donor to the face of the porphyrin opposite the fullerene unit. As the secondary donor, we have chosen two electron-rich phenothiazine derivatives, phenothiazine (PTZ) and 2-methylthiophenothiazine (TPTZ) with appended pyridine

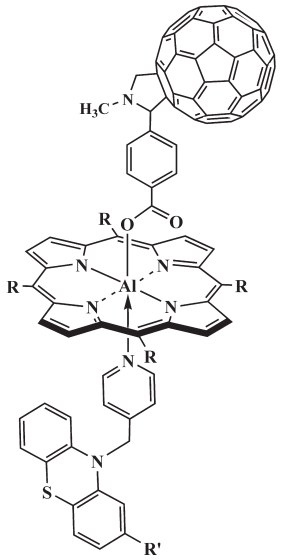

R=Phenyl, R'= H (**PTZpyAlPor-C_{60}**), SCH_3 (**TPTZpyAlPor-C_{60}**)

Figure 1. Structure of the vertical supramolecular triads investigated in this study.

that allows them to coordinate to Al(III). The structures of the two triads (PTZpy→AlPor−C_{60}, TPTZpy→AlPor−C_{60}) are shown in Figure 1, and they are designed such that AlPor is the primary electron donor, fullerene acts as the primary electron acceptor, and the pyridine-appended phenothiazine derivative (PTZpy or TPTZpy) acts as the secondary electron donor. The choice of PTZpy or TPTZpy as the secondary donor is motivated by the fact that the first oxidation potentials of phenothiazines are close to that of AlPor, which minimizes energy loss during the secondary electron transfer. Time-resolved spectroscopy reveals that the triads depicted in Figure 1 undergo light-induced multistep electron transfer. We will show that the stabilization of the charge separation by the secondary electron transfer is relatively modest and discuss possible reasons for this in terms of the electronic coupling.

2. EXPERIMENTAL SECTION

2.1. Steady-State Characterization Methods. ^{1}H NMR spectra were recorded with a Bruker Avance 300 Digital NMR spectrometer using $CDCl_3$ as the solvent. FAB mass spectra were recorded on a Kratos Concept 1S high-resolution E/B mass spectrometer and Bruker Autoflex TOF/TOF MALDI spectrometer. The UV/vis spectra were recorded with a ThermoSpectronic/Unicam UV-4 UV−vis spectrometer. Cyclic and differential pulse voltammetric experiments were performed in *o*-dichlorobenzene (*o*-DCB) containing 0.1 M tetrabutylammoniumperchlorate (TBAP) on a BAS Epsilon electrochemical analyzer (working electrode: glassy carbon, auxiliary electrode: Pt wire; reference electrode: Ag). The Fc^+/Fc (Fc = ferrocene) couple was used to calibrate the redox potential values. Steady-state emission spectra were recorded using a Photon Technologies International (London, Ontario) Quanta Master Model QM-2001 L-format, equipped with double-grating monochromators and a 150 W xenon lamp, running Felix 32 software.

2.2. Absorbance and Fluorescence Titrations. Absorption titrations were carried out in *o*-DCB at concentrations appropriate for measuring the Soret band. A solution containing the

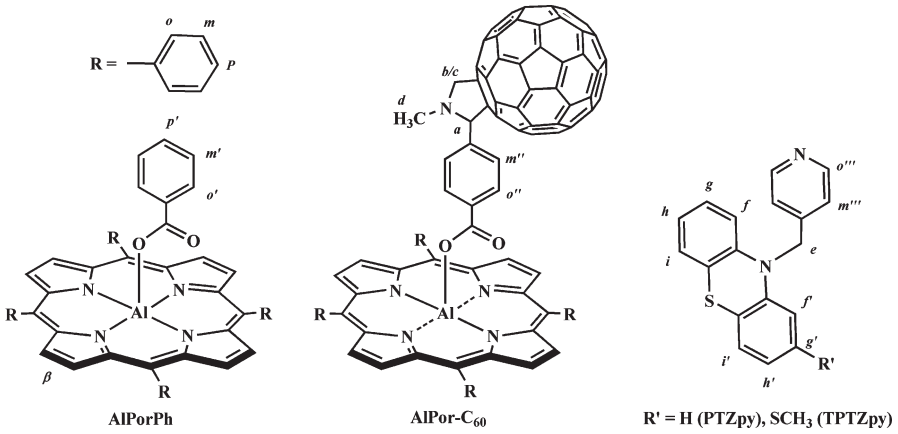

Figure 2. Structures of the components of the triads and reference compound.

acceptor (A = AlPorPh or AlPor−C_{60}) was placed in a cuvette and titrated by adding aliquots of a concentrated solution of the donor (D = py, PTZpy, or TPTZpy). The donor solution also contained the acceptor at its initial concentration so that the porphyrin concentration remained constant throughout the titration. The binding constants were calculated using the Benesi−Hildebrand equation,[55] $[A]/Abs = (1/[D])(1/\varepsilon K) + (1/\varepsilon)$, where [A] is the total concentration of bound and unbound acceptor and is kept fixed, Abs is the absorbance of the complex at the wavelength λ, [D] is the total concentration of the donor which is varied, K = binding constant, and ε is the molar absorptivity of the D−A complex at the excitation wavelength λ. In an analogous manner, steady-state fluorescence titrations were carried out in *o*-DCB using solutions at constant concentration of acceptor and varying concentration of donor. The solutions were excited at the isosbestic point wavelength, obtained from the absorption titrations. The binding constant (K) was calculated using the Benesi−Hildebrand equation, $I_0/(I_0 - I) = (1/[D])(1/\varepsilon K) + (1/\varepsilon)$, where I_0 and I represent the fluorescence intensity in the absence and presence of donor unit, respectively, ε is the fluorescence quenching or enhancement factor, and K is the binding constant.

2.3. Transient EPR Spectroscopy. Transient EPR time/field data sets were recorded using a modified Bruker EPR 200D-SRC X-band spectrometer (Bruker Canada, Milton ON, Canada). Light excitation at 532 nm was achieved using 10 ns pulses from a Nd:YAG laser at a repetition rate of 10 Hz. EPR samples were prepared by dissolving the porphyrin complex under study in the *o*-DCB to a concentration of $\sim 10^{-4}$ M. The solutions were placed in suprasil EPR sample tubes (4 mm o.d.) and were degassed by several freeze−pump−thaw cycles and then sealed under vacuum.

2.4. Time-Resolved Fluorescence Spectroscopy. Time-resolved fluorescence decays were measured using the single photon counting method and a streakscope (Hamamatsu Photonics, C5680) as a detector and a laser (Hamamatsu Photonics M10306, laser diode head, 408 nm) as an excitation source. Lifetimes were evaluated with software included in the apparatus.

2.5. Transient Optical Difference Spectroscopy. Nanosecond transient absorption measurements were carried out using the second harmonic (532 nm) of a Nd:YAG laser (Spectra-Physics, Quanta-Ray GCR-130, 5 ns fwhm) as an excitation source. For transient absorption spectra in the near-IR region (600−1200 nm) and the time profiles, monitoring light from a pulsed Xe lamp was detected with a Ge-APD (Hamamatsu Photonics, B2834). For the measurements in the visible region (400−1000 nm), a Si-PIN photodiode (Hamamatsu Photonics, S1722-02) was used as a detector.

3. RESULTS AND DISCUSSION

3.1. Preparation of the Phenothiazine−Aluminum(III) Porphyrin−Fullerene Triads. The triads shown in Figure 1 have been assembled from the components AlPor−C_{60}, PTZpy (and TPTZpy) shown in Figure 2. Also shown in Figure 2 is the porphyrin reference compound AlPorPh. We have reported the synthesis and characterization of the AlPor−C_{60} dyad previously.[48] The fullerene moiety is covalently attached to the aluminum porphyrin via a benzoate linkage formed by condensation of the hydroxy porphyrin and benzoic acid functionalized fullerene. The pyridine-appended phenothiazine derivatives PTZpy and TPTZpy were prepared according to literature methods[10,56,57] (see Supporting Information for details). Coordination of PTZpy or TPTZpy with AlPor−C_{60} affords the axial triads shown in Figure 1. The formation of the triad was followed by ^{1}H and ^{1}H−^{1}H COSY NMR (see Supporting Information, Figure S3), UV/vis absorbance, and steady-state fluorescence studies.

3.2. NMR Spectra. Figure 3 shows the ^{1}H NMR spectrum of a 1:1 mixture of AlPor−C_{60} and PTZpy (top) along with the individual spectra of AlPor−C_{60} (middle) and PTZpy (bottom). In the coordination complex, shielding due to the porphyrin ring causes an upfield shift of the PTZpy protons on the pyridine unit (o''' and m'''), bridging methylene group (e), and PTZ moiety (f and f'), as indicated by the dashed lines in Figure 3. The magnitude of the shift depends on the distance of the protons from the porphyrin ring, and the pyridinyl protons (o''' and m''') display the greatest shift indicating that coordination occurs via the pyridinyl group. On the benzoate bridging group to the fullerene, the protons closest to the porphyrin ring (o'') show an increased upfield shift upon coordination, suggesting that the aluminum(III) center lies out of the porphyrin plane in AlPor−C_{60} and is pulled into the plane when PTZpy coordinates. Similar results were obtained for complexation of AlPor−C_{60} with TPTZpy.

3.3. Absorption Spectra and Titrations. Figure 4 shows the absorption spectra of the components of the self-assembled triads measured in dichloromethane. The spectrum of the covalently bound dyad AlPor−C_{60} is essentially a superposition of the spectra of the porphyrin and fullerene reference compounds AlPorPh and

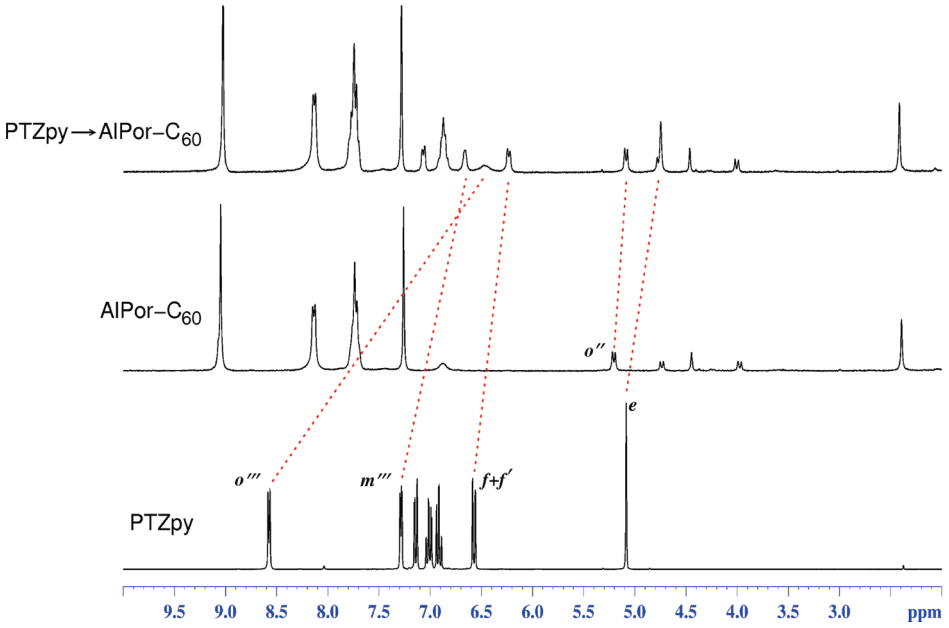

Figure 3. ^{1}H NMR (300 MHz) spectra of 2.9 mM solutions of PTZpy→AlPor−C_{60}, AlPor−C_{60}, and PTZpy in $CDCl_3$. The peak labels refer the structures in Figure 2.

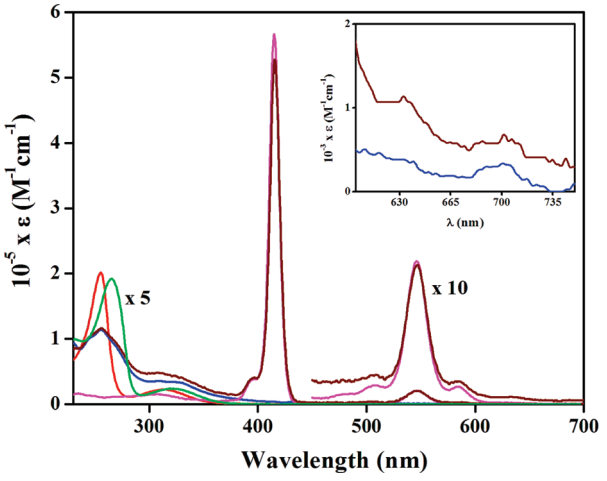

Figure 4. UV−visible absorption spectra of PTZpy (red), TPTZpy (green), C_{60}COOMe (blue), AlPorPh (magenta), and AlPor−C_{60} (wine) in dichloromethane. The inset shows weak long-wavelength fullerene absorption bands.

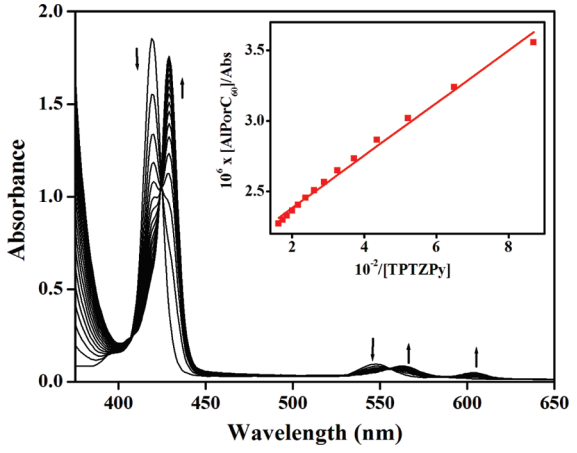

Figure 5. Absorption titration of AlPor−C_{60} with TPTZpy in *o*-DCB. The inset shows the Benesi−Hildebrand plot of the change of absorbance at 429 nm. TPTZpy was added up to 6.2 × 10^{-3} M in 3.85 × 10^{-4} M increments to a 4 × 10^{-6} M solution of AlPor−C_{60}.

C_{60}COOMe. The porphyrin shows the typical strong Soret band and weak Q-band at 416 and 547 nm, respectively. The fullerene unit has moderately strong $\pi-\pi^*$ absorption bands in the UV region with maxima at 275 and 325 nm and weak absorption bands in the visible region at 430 and 700 nm. The spectrum of AlPor−C_{60} has a weak tail at long wavelength (Figure 4, inset), which has been suggested to arise from a weak charge-transfer interaction between the porphyrin and fullerene in related complexes.[58,59] The pyridine-appended phenothiazine derivatives PTZpy and TPTZpy have relatively weak absorption maxima at 256, 314 nm and 266, 322 nm, respectively.

Figure 5 shows absorption titrations of AlPor−C_{60} with TPTZpy in *o*-DCB. Upon adding TPTZpy, the Soret band of the porphyrin shifts from 419 to 429 nm and the Q-bands at 547 and 583 nm are shifted to 563 and 603 nm. Isosbestic points are observed at 424 and 555 nm, indicating the formation of a complex between AlPor−C_{60} and TPTZpy, and the shifts in the porphyrin bands are typical of axial coordination of nitrogen ligands to aluminum(III) porphyrins.[51] Benesi−Hildebrandt analysis[55] (Figure 5, inset) gives a linear plot indicating that a 1:1 complex is formed, and the slope yields a binding constant $K = 1.1 \times 10^3$ M^{-1} showing that the supramolecular triad has a high degree of stability. The *K* values of pyridine, PTZpy and TPTZpy to AlPor−C_{60} and AlPorPh are summarized in Table 1 and are roughly the same for all six of the complexes. Thus, substitution of the benzoate and pyridine moieties with C_{60} and PTZ does not greatly affect the binding, which suggests that this binding motif could be used to attach a variety of donors and acceptors to the porphyrin.

3.4. Fluorescence Titrations. Figure 6 shows the fluorescence spectra of the AlPor−C_{60} dyad with increasing amounts of pyridine-appended phenothiazine (TPTZpy). The excitation

Table 1. Absorption Wavelength (λ_{max}, nm) and Binding Constants (K, M^{-1}) in *o*-DCB

sample	λ_{max} (nm)	K (M^{-1})
AlPorPh	419, 548, 587	–
py→AlPorPh	429, 562, 603	1.1×10^3
PTZpy→AlPorPh	429, 562, 603	1.1×10^3
TPTZpy→AlPorPh	429, 563, 603	1.0×10^3
AlPor−C_{60}	419, 548, 583	–
py→AlPor−C_{60}	429, 560, 603	1.2×10^3
PTZpy→AlPor−C_{60}	429, 562, 604	1.3×10^3
TPTZpy→AlPor−C_{60}	429, 563, 603	1.2×10^3

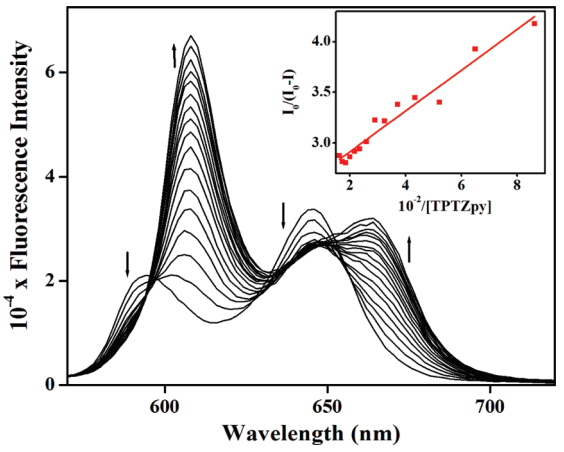

Figure 6. Fluorescence titrations of AlPor−C_{60} with TPTZpy in *o*-DCB. The excitation wavelength was chosen at the isosbestic point, 556 nm, obtained from UV−visible titrations. TPTZpy was added in 3.85×10^{-4} M increments to a 4×10^{-6} M solution of AlPor−C_{60}. The inset shows the Benesi−Hildebrand plot constructed by monitoring the emission intensity at the 592 nm band for calculating the binding constant. The abbreviations I_0 and I represent fluorescence intensity in the absence and presence of TPTZpy, respectively.

wavelength was adjusted to the isosbestic point at 556 nm so that the extinction coefficient is the same for each sample solution. In the absence of TPTZpy, the fluorescence spectrum of the AlPor−C_{60} dyad shows peaks at 595 and 645 nm similar to those of AlPor. However, the intensities are much decreased due to the charge separation from the excited singlet state of AlPor to axial C_{60}.[48] Upon addition of TPTZpy, the fluorescence peaks shift to longer wavelengths (see Table 2), and the relative fluorescence intensities change with isosbestic points at 595, 630, and 655 nm, supporting formation of a coordination complex, TPTZpy→AlPor−C_{60}. Similar results were observed for the titration of pyridine and PTZpy with AlPor−C_{60}, which indicates that the changes in the spectrum are a result of the binding of the pyridine moiety and not the presence of phenothiazine as an electron donor.

To calculate the binding constant of TPTZpy with AlPor−C_{60}, the fluorescence data were also analyzed using the Benesi−Hildebrand method, which yielded a linear plot indicating a 1:1 complex formation (Figure 6, inset) and a binding constant $K = 1.2 \times 10^3$ M^{-1}. The magnitude of the binding constant is identical to that obtained from absorption titrations. Similar results were observed from titrations of the reference compound AlPorPh with TPTZpy. However the enhancement in fluorescence intensity varies in the different complexes. The origin of

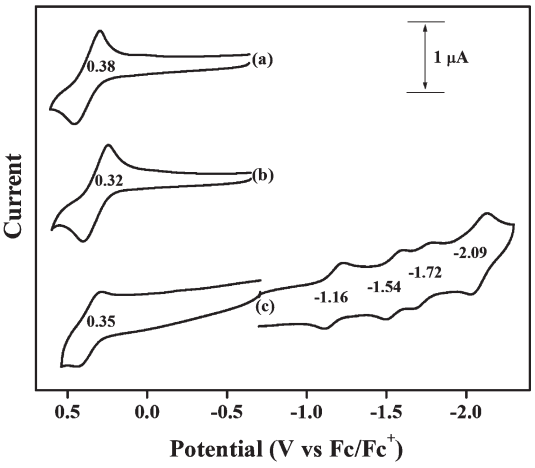

Figure 7. Cyclic voltammograms of (a) 0.3 mM PTZpy, (b) 0.3 mM TPTZpy, and (c) 0.3 mM AlPor−C_{60} in 0.1 M TBAP, *o*-DCB. Scan rate = 100 mV/s. The oxidation and reduction midpoint potentials obtained from the voltammograms are indicated.

these differences is unclear, but, in principle, they could be caused by the structural changes that lead to the red shift of the absorption and emission bands of the porphyrin ring and/or by electron transfer.

3.5. Redox Potential Measurements and Energy Diagrams of the Triads. To evaluate the energetic schemes of electron transfer in the triads, cyclic voltammograms and redox data of PTZpy, TPTZpy, and AlPor−C_{60} were obtained and are shown in Figure 7. The energies of the possible charge-separated radical ion pairs (E_{RIP}) are calculated as the difference of the appropriate oxidation and reduction potentials. The stabilization energy due to the Coulomb interaction of the charges will lower the actual E_{RIP} somewhat compared to these values. The energies of the aluminum porphyrin excited singlet state (E_S) and triplet state (E_T) are estimated from the blue edge of the fluorescence spectra (Figure 6) at 580 nm (2.14 eV) and phosphorescence spectra (Figure S4) at 788 nm (1.57 eV), respectively. The singlet and triplet energies for fullerene, 1.75 and 1.50 eV, respectively, have been taken from the literature.[38] The free energy change for the initial charge separation giving AlPor$^{\bullet+}$−$C_{60}^{\bullet-}$ is calculated from the radical ion pair and singlet state energies using the simplified Rehm−Weller equation $\Delta G_{CS} = E_{RIP} - E_S$.[60,61] The driving force (ΔG_{HS}) of the hole shift from AlPor$^{\bullet+}$ to the secondary electron donor PTZ or TPTZ is estimated from the difference of the ion pair energies. These calculated free energy changes are summarized in Table 3. For the initial charge separation from ^{1}AlPor* to C_{60}, we obtain a value of at least −0.60 eV for the driving force ($\Delta G_{CS}(^1\text{AlPor}^* \rightarrow \text{AlPor}^{\bullet+}-C_{60}^{\bullet-})$), indicating that the activation energy for this process will likely be fairly small since the reorganization energy is expected to be roughly 0.50−0.60 eV[29,41,46,62,63] and thus of similar magnitude but of opposite sign to ΔG_{CS}. On the other hand, the free energy change ΔG_{HS} for the hole shift from AlPor$^{\bullet+}$ to the secondary electron donor PTZ or TPTZ is found to be essentially zero. Since the Coulomb stabilization should be larger in AlPor$^{\bullet+}$−$C_{60}^{\bullet-}$ than in PTZ$^{\bullet+}$→AlPor−$C_{60}^{\bullet-}$, it is likely that the hole shift is slightly endergonic. Regardless of the sign of ΔG_{HS}, its magnitude is small, and therefore the activation energy and the rate of the hole shift will be determined largely by the reorganization energy. Figure 8 shows the energy diagram for the triads. As can be seen in Figure 8, the radical ion pairs are similar in energy to the triplet states, ^{3}AlPor*−C_{60} and AlPor−$^3C_{60}$*, which suggests that singlet−triplet mixing in the

dx.doi.org/10.1021/jp110156w |*J. Phys. Chem. A* 2011, 115, 709–717

Table 2. Fluorescence Maxima (λ_F), Lifetimes (τ_F), and Quenching Rate Constants (k_q^S)[a]

sample[b]	λ_F/nm[c]	τ_F/ps (A)[d]	k_q^S/s^{-1} ($\Phi_q^S \times A$)	k_{CR}/s^{-1} (τ_{RIP}/ns)
AlPorPh	594, 646	7050 (1.00)	–	–
PTZpy→AlPorPh	610, 663	7000 (1.00)	1.0×10^6	–
TPTZpy→AlPorPh	610, 663	6900 (1.00)	3.1×10^6	–
AlPor−C_{60}	594, 646	2900 (0.10), 210 (0.90)	4.6×10^9 (0.97 × 0.90)	2.54×10^7 (39)
py→AlPor−C_{60}	607, 662	2820 (0.11), 205 (0.89)	4.7×10^9 (0.97 × 0.89)	2.60×10^7 (38)
PTZpy→AlPor−C_{60}	609, 662	2550 (0.12), 198 (0.88)	4.9×10^9 (0.97 × 0.88)	1.00×10^7 (100)
TPTZpy→AlPor−C_{60}	609, 665	2120 (0.08), 182 (0.92)	5.4×10^9 (0.97 × 0.92)	1.20×10^7 (83)

[a] Emission maxima (λ_F), fluorescence lifetimes (τ_f), relative amplitude of the decay component (A), singlet state quenching rate constant (k_q^S), quantum yield of the quenching process (Φ_q^S), charge recombination rate constant (k_{CR}), and radical ion pair lifetime (τ_{RIP}) calculated from the decay of the 1020 nm band. [b] In *o*-DCB solution. [c] λ_{exc} = ~555 nm. [d] λ_{exc} = 406 nm. $k_q^S = (1/\tau_F)_{sample} - (1/\tau_F)_{reference}$, $\Phi_q^S = [(1/\tau_F)_{sample} - (1/\tau_F)_{reference}]/(1/\tau_F)_{sample}$.

radical pair and triplet recombination may contribute to the overall lifetime of the charge separation.

3.6. Transient EPR Spectroscopy. In the soft glass of *o*-DCB at 200 K, the transient EPR (TREPR) spectra of AlPor−C_{60} and PTZpy→AlPor−C_{60} show weak narrow features consistent with a radical pair superimposed on the C_{60} triplet spectrum (Figure S5).[48] The polarization pattern of the C_{60} triplet state indicates that it is populated by intersystem crossing and not by radical pair recombination. In frozen solution in *o*-DCB, cw EPR experiments reveal the accumulation of light-induced stable radicals, but TREPR measurements show only the triplet state of C_{60} (data not shown). At room temperature in the liquid crystal 5CB, only weak signals from the triplet state of C_{60} are observed by TREPR (Figure S5). However, the absence of a radical pair spectrum under these conditions could be due to either fast spin relaxation, motional averaging of the spectrum, and/or a short lifetime of the radical pair. Thus, the EPR data show that light excitation of the dyad and triads results in population of the C_{60} triplet state by intersystem crossing and give some evidence for light-induced charge separation in the soft glass and solid.

3.7. Time-Resolved Fluorescence Spectroscopy. Time profiles in the AlPor fluorescence region measured using single photon counting are shown in Figure 9. As can be seen, the presence of the C_{60} in AlPor−C_{60} (blue curve) decreases the fluorescence lifetime (τ_F) dramatically compared with AlPorPh (black curve). Complexation of AlPor−C_{60} with PTZpy (green curve) and TPTZpy (red curve) leads to an additional small decrease in the fluorescence lifetime. The fluorescence traces from AlPor−C_{60} and its complexes (PTZpy→AlPor−C_{60} and TPTZpy→AlPor−C_{60}) are biexponential with a major short-lived component ($\tau_F \approx 200$ ps) and a minor long-lived component ($\tau_F \approx 2$ ns) that accounts for at most 12% of the intensity, while those from AlPorPh and its complexes (PTZpy→AlPorPh and TPTZpy→AlPorPh) decay monoexponentially with a lifetime of $\tau_F \approx 7$ ns (see Supporting Information Figure S6). The values of τ_F are summarized in Table 2. From the difference of the τ_F values for (Donor)py→AlPor−C_{60} and that of AlPorPh, the quenching rate constants (k_q^S) and quantum yield (Φ_q^S) were calculated as listed in Table 2. If charge separation and energy transfer to C_{60} are assumed to be responsible for the fluorescence quenching, the quenching rate constant is given by $k_q^S = k_{CS}^S + k_{EnT}^S$. However, since no fluorescence from C_{60} is observed in the 700−750 nm region in Figure 6, the energy-transfer rate must be small and $k_q^S \approx k_{CS}^S \approx 5 \times 10^9$ s^{-1}. Thus, the data suggest that charge separation between AlPor and C_{60} takes place predominantly with time constant of about 200 ps. The fact that complexation of AlPor−C_{60} with the PTZpy and TPTZpy secondary donors causes only small changes in the lifetimes suggests that (i) the rates and yields of electron transfer from AlPor to C_{60} are roughly the same in all of the complexes and (ii) electron transfer from PTZpy and TPTZpy to the excited singlet state of AlPor is too slow to compete with electron transfer from AlPor to C_{60}. The observed slight decrease in τ_F suggests that coordination by PTZpy and TPTZpy may cause a slight increase in the ability of AlPor to act as an electron donor. The fluorescence data do not give any clear indication of whether secondary electron transfer from PTZpy and TPTZpy to AlPor$^{\bullet+}$ takes place. However, this question can be addressed using nanosecond transient absorption spectroscopy.

3.8. Transient Absorption Spectroscopy. Figure 10 shows a comparison of the transient absorption difference spectra of the triad PTZpy→AlPor−C_{60} and the reference complex py→AlPor−C_{60} measured in Ar-saturated *o*-DCB solution at room temperature using 532 nm laser light to excite mainly the porphyrin unit. Formation of $C_{60}^{\bullet-}$ is known to give a characteristic peak at 1000−1200 nm and weaker absorbance changes at 550−600 nm[64−66], while formation of $^3C_{60}$* results in a strong peak at 700−720 nm.[67] The absorption spectrum of PTZ$^{\bullet+}$ has a prominent peak at 600 nm[68], while ^{3}AlPor* has a strong maximum at 500 nm and a weaker peak at 820 nm,[48] and the small absorption changes due to AlPor$^{\bullet+}$ are anticipated in the 600−650 nm region.[48] All three spectra in Figure 10 show peaks due to $^3C_{60}$* and ^{3}AlPor* at 500, 700, and 820 nm. The characteristic peak due to $C_{60}^{\bullet-}$ is clearly visible at 1020 nm in the transient absorption spectra of py→AlPor−C_{60} and AlPor−C_{60}, suggesting the formation of py→AlPor$^{\bullet+}$−$C_{60}^{\bullet-}$ and AlPor$^{\bullet+}$−$C_{60}^{\bullet-}$, although the absorption due to AlPor$^{\bullet+}$ is obscured by the bleaching of the Q-band at 580 nm and absorption of $^3C_{60}$* at 700 nm. The time profile at 1020 nm for PTZpy→AlPor−C_{60}, shown as an inset in Figure 10, decays more slowly than those of py→AlPor−C_{60} and AlPor−C_{60} and yields a first-order rate constant of 1.0×10^7 s^{-1} for the decay of $C_{60}^{\bullet-}$; a similar value of 1.2×10^7 s^{-1} is obtained for TPTZpy→AlPor−C_{60}, (see Supporting Information Figure S10). These rate constants are smaller by a factor of about 3 than the corresponding rate constant of 3×10^7 s^{-1} obtained for py→AlPor−C_{60} and AlPor−C_{60} and can be attributed to the charge recombination (k_{CR}), regardless of where the hole center resides.

Furthermore, careful comparison of the spectrum of PTZpy→AlPor−C_{60} with that of py→AlPor−C_{60} shows that the PTZ complex has additional peaks at 520 and 600 nm, which we assign to PTZ$^{\bullet+}$. In control experiments with PTZpy→AlPorPh and TPTZpy→AlPorPh (see Supporting Information Figures S7 and S8), no evidence for charge separation was found in the nanosecond time region.

Table 3. Charge-Separated State Energies (E_{RIP}, eV), Free Energy Changes of Electron Transfer ($-\Delta G_{CS}$, eV), and the Hole Shift ($-\Delta G_{HS}$, eV) in the Triads in *o*-DCB[a]

sample	E_{RIP}, eV (AlPor$^{\bullet+}$−C$_{60}^{\bullet-}$)	E_{RIP}, eV (PTZ$^{\bullet+}$−C$_{60}^{\bullet-}$)	E_{RIP}, eV (PTZ$^{\bullet+}$−AlPor$^{\bullet-}$)	$-\Delta G_{CS}$, eV (^{1}AlPor*→AlPor$^{\bullet+}$−C$_{60}^{\bullet-}$)	$-\Delta G_{HS}$, eV (AlPor$^{\bullet+}$−C$_{60}^{\bullet-}$→PTZ$^{\bullet+}$−C$_{60}^{\bullet-}$)
AlPor−C$_{60}$	1.51	−	−	0.60	−
PTZpy→AlPor−C$_{60}$	1.51	1.54	2.10	0.60	−0.03
TPTZpy→AlPor−C$_{60}$	1.51	1.48	2.04	0.60	0.03

[a] $\Delta G_{CS} = E_{RIP} - E_S$, $E_{RIP} = e[E_{1/2}(D^{\bullet+}/D) - E_{1/2}(A/A^{\bullet-})]$, where $E_{1/2}(D^{\bullet+}/D)$ is the first oxidation potential of the donor, $E_{1/2}(A/A^{\bullet-})$ is the first reduction potential of the acceptor, E_S is the singlet state energy of aluminum(III) porphyrin (2.14 eV). $\Delta G_{HS} = E_{RIP}$(AlPor$^{\bullet+}$−C$_{60}^{\bullet-}$) − E_{RIP}(PTZ$^{\bullet+}$py→AlPor−C$_{60}^{\bullet-}$ or TPTZ$^{\bullet+}$py→AlPor−C$_{60}^{\bullet-}$). $\Delta G_{CR} = -e[E_{1/2}(D^{\bullet+}/D) - E_{1/2}(A/A^{\bullet-})]$.

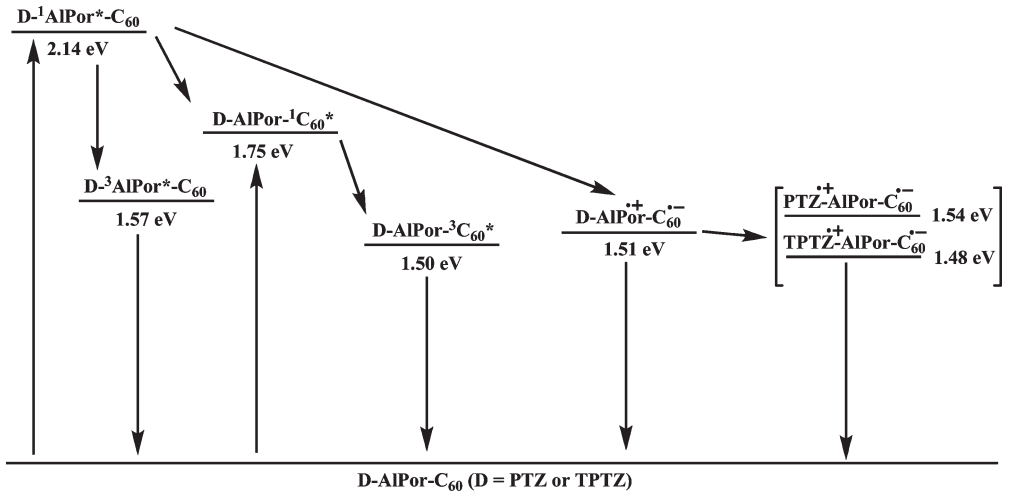

Figure 8. Energy level diagram of the newly constructed triads.

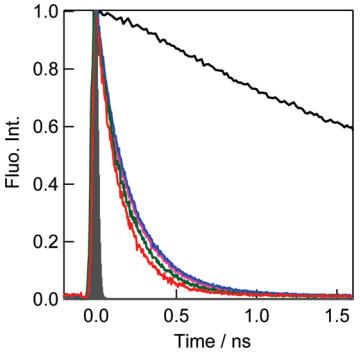

Figure 9. Fluorescence decay (λ_{exc} = 408 nm, λ_{em} = 600−700 nm) profiles of 0.1 mM AlPorPh (black), AlPor−C$_{60}$ (blue), py→AlPor−C$_{60}$ (pink), PTZpy→AlPor−C$_{60}$ (green), and TPTZpy→AlPor−C$_{60}$ (red) in *o*-DCB. For PTZpy→AlPor−C$_{60}$ and TPTZpy→AlPor−C$_{60}$, the respective pyridine derivative was added in a 2:1 mol ratio to AlPor−C$_{60}$.

Together, the fluorescence and transient absorption data point to the occurrence of primary charge separation from the excited singlet state of the porphyrin to the fullerene unit. The observation of absorbance changes associated with PTZ$^{\bullet+}$ suggests that the initial charge separation is followed by a hole shift from AlPor$^{\bullet+}$ to PTZ giving the final charge-separated state, PTZ$^{\bullet+}$py→AlPor−C$_{60}^{\bullet-}$. The absorbance changes associated with C$_{60}^{\bullet-}$ and PTZ$^{\bullet+}$ appear within the 8 ns excitation laser pulse width, which determines the spectrometer time resolution, indicating that the initial charge separation and the hole shift occur within this time. Together with the observed fluorescence lifetime of ~200 ps, the fact that PTZ$^{\bullet+}$ is present within 8 ns suggests that the hole shift occurs with a lifetime of a few nanoseconds, following electron transfer from ^{1}AlPor* to C$_{60}$ in ~200 ps. The decay rates of the absorption changes at 520 nm (Figure S9) and 1020 nm are essentially the same; hence, we assign the decay to charge recombination in PTZ$^{\bullet+}$py→AlPor−C$_{60}^{\bullet-}$.

3.9. Sequential Electron Transfer. The secondary donor is designed to kinetically stabilize the charge separation by donation of an electron to the oxidized primary donor. For this process to be effective, the hole shift must be faster than recombination in the initial charge-separated state and the overall lifetime of the charge-separated state should be prolonged by formation of the secondary charge-separated state. The transient absorbance and fluorescence data indicate that electron donation to AlPor$^{\bullet+}$ from PTZ (or TPTZ) occurs within a few nanoseconds and thus is about an order magnitude faster than the lifetime of AlPor$^{\bullet+}$−C$_{60}^{\bullet-}$ (τ_{RIP}, see Table 2). The overall τ_{RIP} is increased by roughly a factor of ~2.5 from 39 ns in AlPor−C$_{60}$ to 100 ns in PTZpy→AlPor−C$_{60}$ (and 83 ns in TPTZpy→AlPor−C$_{60}$). Control experiments with py→AlPor−C$_{60}$ show that coordination with pyridine has no effect on the recombination rate confirming that the increased τ_{RIP} values in the triads are indeed due to the hole shift to PTZ (or TPTZ). The fact that the back reaction is slightly faster with TPTZ than with PTZ as the secondary donor may be due to slight differences in their midpoint potentials and hence in the driving force for recombination.

3.10. Electronic Coupling in the Axial Direction. One of the motivations for constructing the triads was to investigate the influence of axial binding on the electronic coupling between

dx.doi.org/10.1021/jp110156w |*J. Phys. Chem. A* 2011, 115, 709–717

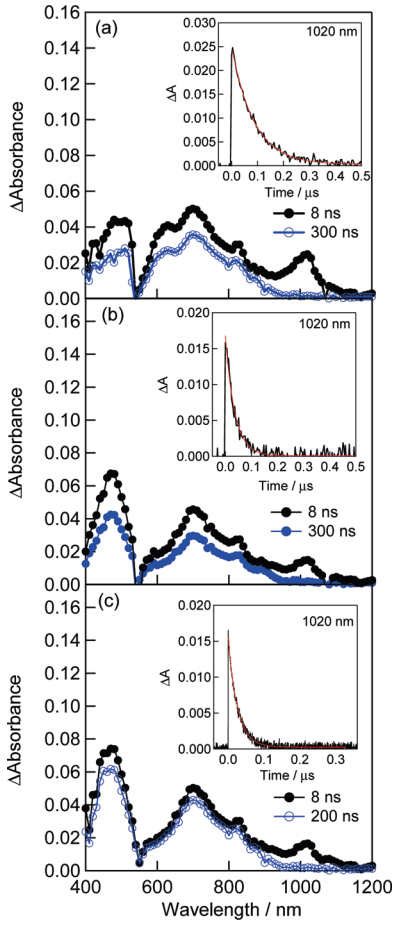

Figure 10. Nanosecond transient absorption spectra of 0.1 mM (a) PTZpy→AlPor−C_{60}, (b) 0.1 mM py→AlPor−C_{60} (ratio of py: AlPor−C_{60}, 2:1), and (c) 0.1 mM AlPor−C_{60} observed by 532 nm (ca. 3 mJ/pulse) laser-light irradiation in Ar-saturated *o*-DCB. Inset: Absorption−time profiles at 1020 nm.

porphyrin and electron-transfer components. Recently, Marcus curves have been determined for electron transfer in the axial direction in a series of silicon phthalocyanine (SiPc) triads[69] and in the horizontal direction in a zinc porphyrin fullerene dyad (ZnP−C_{60}).[41] From these Marcus curves, it was found that the electronic coupling in the axial phthalocyanine complexes (70 cm^{-1}) was much larger than in ZnP−C_{60} (3.9 cm^{-1}). The charge separation and recombination rates and corresponding ΔG values between AlPor and C_{60} ($k_{CS} \sim 5 \times 10^9$ s^{-1}, $\Delta G_{CS} = -0.60$ eV) ($k_{CR} \sim 3 \times 10^7$ s^{-1}, $\Delta G_{CR} = -1.51$ eV) determined here lie relatively close to the ZnP−C_{60} Marcus curve[41] but are far removed from that of the SiPc triads[69] suggesting that the electronic coupling between AlPor and C_{60} is similar to the value found for ZnP and C_{60}. Thus, the placement of the fullerene in the axial position or in the porphyrin plane does not appear to have a large effect on the electronic coupling.

The observation that the hole shift occurs rapidly, despite the expected large activation energy for this step, suggests that coupling between AlPor and PTZ (or TPTZ) may be slightly stronger than between AlPor and C_{60}. However, the rate of the hole shift depends critically on the reorganization energy, and we do not have enough data at present to accurately estimate this coupling. The increase in τ_{CR} resulting from the addition of the secondary donor is relatively modest, even though the distance between C_{60} and PTZ (or TPTZ) is roughly twice as large as between AlPor and C_{60}, suggesting that the final charge recombination occurs directly in one step, that is, via the superexchange mechanism rather than stepwise.

4. CONCLUSIONS

The triads presented here demonstrate that sequential charge separation along a direction axial to the porphyrin ring is possible. With the chosen ligands, the secondary electron transfer provides a modest stabilization of the charge separation. It is notable that the lifetime of the radical ion pair (τ_{RIP}) in the two triads is significantly longer than the value of τ_{RIP} = 18 ns found for the related triad ferrocene−AlPor−C_{60}[48] in which the secondary donor is attached to the periphery of the porphyrin ring because ferrocene with a low-lying triplet state provides an additional path to for rapid recombination of the RIP with triplet spin character.[66] We are currently exploring other secondary donors and alternative bridging groups to extend the lifetime of the axial charge separation.

■ ASSOCIATED CONTENT

Supporting Information. Details of synthesis, NMR spectra, phosphorescence spectrum of aluminum(III) porphyrin, transient EPR spectra, fluorescence decay profiles, and transient absorption spectra. This material is available free of charge via the Internet at http://pubs.acs.org.

■ AUTHOR INFORMATION

Corresponding Author
*E-mail: avde@brocku.ca (A.v.d.E.); ito@tagen.tohoku.ac.jp (O.I.).

■ ACKNOWLEDGMENT

This work was supported by the National Sciences and Engineering Research Council Canada (P.P.K. and A.v.d.E.) and a JSPS fellowship (A.S.D.S.). This work was partially supported by Grant-in-Aid for Scientific Research (No. 21710104 to T.H.) from MEXT, Japan. We thank Professor H. Murata of JAIST, Japan, for his help.

■ REFERENCES

(1) Meyer, T. J. *Acc. Chem. Res.* **1989,** *22,* 163.
(2) Gust, D.; Moore, T. A. *Top. Curr. Chem.* **1991,** *159,* 103.
(3) Wasielewski, M. R. *Chem. Rev.* **1992,** *92,* 435.
(4) Gust, D.; Moore, T. A.; Moore, A. L. *Acc. Chem. Res.* **2001,** *34,* 40.
(5) Sun, L. C.; Hammarstrom, L.; Akermark, B.; Styring, S. *Chem. Soc. Rev.* **2001,** *30,* 36.
(6) Wasielewski, M. R. *J. Org. Chem.* **2006,** *71,* 5051.
(7) Gust, D.; Moore, T. A.; Moore, A. L. *Acc. Chem. Res.* **2009,** *42,* 1890.
(8) Hasobe, T. *Phys. Chem. Chem. Phys.* **2010,** *12,* 44.
(9) Marcus, R. A.; Sutin, N. *Biochim. Biophys. Acta* **1985,** *811,* 265.
(10) Collin, J. P.; Guillerez, S.; Sauvage, J. P.; Barigelletti, F.; Decola, L.; Flamigni, L.; Balzani, V. *Inorg. Chem.* **1991,** *30,* 4230.
(11) Curiel, D.; Ohkubo, K.; Reimers, J. R.; Fukuzumi, S.; Crossley, M. J. *Phys. Chem. Chem. Phys.* **2007,** *9,* 5260.
(12) Imahori, H. *Org. Biomol. Chem.* **2004,** *2,* 1425.
(13) Imahori, H.; Mori, Y.; Matano, Y. *J. Photochem. Photobiol., C* **2003,** *4,* 51.
(14) D'Souza, F.; Chitta, R.; Gadde, S.; Islam, D. M. S.; Schumacher, A. L.; Zandler, M. E.; Araki, Y.; Ito, O. *J. Phys. Chem. B* **2006,** *110,* 25240.

(15) D'Souza, F.; Smith, P. M.; Gadde, S.; McCarty, A. L.; Kullman, M. J.; Zandler, M. E.; Itou, M.; Araki, Y.; Ito, O. *J. Phys. Chem. B* **2004,** *108,* 11333.
(16) Winters, M. U.; Dahlstedt, E.; Blades, H. E.; Wilson, C. J.; Frampton, M. J.; Anderson, H. L.; Albinsson, B. *J. Am. Chem. Soc.* **2007,** *129,* 4291.
(17) Nakagawa, H.; Ogawa, K.; Satake, A.; Kobuke, Y. *Chem. Commun.* **2006,** 1560.
(18) Albinsson, B.; Martensson, J. *J. Photochem. Photobiol., C* **2008,** *9,* 138.
(19) Ito, O.; Yamanaka, K. *Bull. Chem. Soc. Jpn.* **2009,** *82,* 316.
(20) Aratani, N.; Kim, D.; Osuka, A. *Acc. Chem. Res.* **2009,** *42,* 1922.
(21) Guldi, D. M. *Chem. Soc. Rev.* **2002,** *31,* 22.
(22) Beletskaya, I.; Tyurin, V. S.; Tsivadze, A. Y.; Guilard, R.; Stern, C. *Chem. Rev.* **2009,** *109,* 1659.
(23) Imahori, H. *J. Phys. Chem. B* **2004,** *108,* 6130.
(24) Kamat, P. V. *J. Phys. Chem. C* **2007,** *111,* 2834.
(25) Kobuke, Y.; Ogawa, K. *Bull. Chem. Soc. Jpn.* **2003,** *76,* 689.
(26) Fujutsuka, M.; Ito, O. In *Handbook of Photochemistry and Photobiology*; Nalwa, H. S., Ed.; American Scientific Publishers: Valencia, CA; 2003; Vol. 2, Organic Photochemistry, p 111.
(27) Electron Transfer in Functionalized Fullerenes. In *Fullerenes: From Synthesis to Optoelectronic Properties*; Guldi, D., Martin, N., Eds.; Kluwer Academic Publishers: Norwell, MA, 2002.
(28) Guldi, D. M. *Chem. Commun.* **2000,** 321.
(29) Imahori, H.; Hagiwara, K.; Akiyama, T.; Aoki, M.; Taniguchi, S.; Okada, T.; Shirakawa, M.; Sakata, Y. *Chem. Phys. Lett.* **1996,** *263,* 545.
(30) Martin, N.; Sanchez, L.; Illescas, B.; Perez, I. *Chem. Rev.* **1998,** *98,* 2527.
(31) Photochemistry of Fullerenes. In *Handbook of Photochemistry and Photobiology*; Nalwa, H. S., Ed.; American Scientific Publishers: Valencia, CA; 2003; Vol. 2, Organic Photochemistry.
(32) D'Souza, F.; Ito, O. *Chem. Commun.* **2009,** 4913.
(33) Liddell, P. A.; Kodis, G.; de la Garza, L.; Moore, A. L.; Moore, T. A.; Gust, D. *J. Phys. Chem. B* **2004,** *108,* 10256.
(34) Kuramochi, Y.; Satake, A.; Itou, M.; Ogawa, K.; Araki, Y.; Ito, O.; Kobuke, Y. *Chem. Eur. J.* **2008,** *14,* 2827.
(35) Kobori, Y.; Shibano, Y.; Endo, T.; Tsuji, H.; Murai, H.; Tamao, K. *J. Am. Chem. Soc.* **2009,** *131,* 1624.
(36) Maligaspe, E.; Tkachenko, N. V.; Subbaiyan, N. K.; Chitta, R.; Zandler, M. E.; Lemmetyinen, H.; D'Souza, F. *J. Phys. Chem. A* **2009,** *113,* 8478.
(37) Carbonera, D.; Di Valentin, M.; Corvaja, C.; Agostini, G.; Giacometti, G.; Liddell, P. A.; Kuciauskas, D.; Moore, A. L.; Moore, T. A.; Gust, D. *J. Am. Chem. Soc.* **1998,** *120,* 4398.
(38) Luo, C.; Guldi, D. M.; Imahori, H.; Tamaki, K.; Sakata, K. *J. Am. Chem. Soc.* **2000,** *122,* 6535.
(39) Imahori, H.; Sekiguchi, Y.; Kashiwagi, Y.; Sato, T.; Araki, Y.; Ito, O.; Yamada, H.; Fukuzumi, S. *Chem. Eur. J.* **2004,** *10,* 3184.
(40) Imahori, H.; Tamaki, K.; Araki, Y.; Sekiguchi, Y.; Ito, O.; Sakata, Y.; Fukuzumi, S. *J. Am. Chem. Soc.* **2002,** *124,* 5165.
(41) Imahori, H.; Tamaki, K.; Guldi, D. M.; Luo, C. P.; Fujitsuka, M.; Ito, O.; Sakata, Y.; Fukuzumi, S. *J. Am. Chem. Soc.* **2001,** *123,* 2607.
(42) Trabolsi, A.; Elhabiri, M.; Urbani, M.; de la Cruz, J. L. D.; Ajamaa, F.; Solladie, N.; Albrecht-Gary, A. M.; Nierengarten, J. F. *Chem. Commun.* **2005,** 5736.
(43) Kim, H. J.; Park, K. M.; Ahn, T. K.; Kim, S. K.; Kim, K. S.; Kim, D. H.; Kim, H. J. *Chem. Commun.* **2004,** 2594.
(44) Fazio, M. A.; Durandin, A.; Tkachenko, N. V.; Niemi, M.; Lemmetyinen, H.; Schuster, D. I. *Chem. Eur. J.* **2009,** *15,* 7698.
(45) Fukuzumi, S.; Honda, T.; Ohkubo, K.; Kojima, T. *Dalton Trans.* **2009,** 3880.
(46) Schuster, D. I.; Cheng, P.; Jarowski, P. D.; Guldi, D. M.; Luo, C. P.; Echegoyen, L.; Pyo, S.; Holzwarth, A. R.; Braslavsky, S. E.; Williams, R. M.; Klihm, G. *J. Am. Chem. Soc.* **2004,** *126,* 7257.
(47) Kojima, T.; Hanabusa, K.; Ohkubo, K.; Shiro, M.; Fukuzumi, S. *Chem. Eur. J.* **2010,** *16,* 3646.
(48) Poddutoori, P. K.; Sandanayaka, A. S. D.; Hasobe, T.; Ito, O.; van der Est, A. *J. Phys. Chem. B* **2010,** *114,* 14348.
(49) Reed, C. A.; Boyd, P. D. W. *Abstr. Pap. Am. Chem. Soc.* **2003,** *226,* U658.
(50) Kumar, P. P.; Maiya, B. G. *New J. Chem.* **2003,** *27,* 619.
(51) Davidson, G. J. E.; Tong, L. H.; Raithby, P. R.; Sanders, J. K. M. *Chem. Commun.* **2006,** 3087.
(52) Richeter, S.; Thion, J.; van der Lee, A.; Leclercq, D. *Inorg. Chem.* **2006,** *45,* 10049.
(53) Aida, T.; Inoue, S. *Acc. Chem. Res.* **1996,** *29,* 39.
(54) Hirai, Y.; Aida, T.; Inoue, S. *J. Am. Chem. Soc.* **1989,** *111,* 3062.
(55) Benesi, H. A.; Hildebrand, J. H. *J. Am. Chem. Soc.* **1949,** *71,* 2703.
(56) Mehta, G.; Sambaiah, T.; Maiya, B. G.; Sirish, M.; Dattagupta, A. *J. Chem. Soc., Perkin Trans. 1* **1995,** 295.
(57) Chen, P. Y.; Westmoreland, T. D.; Danielson, E.; Schanze, K. S.; Anthon, D.; Neveux, P. E.; Meyer, T. J. *Inorg. Chem.* **1987,** *26,* 1116.
(58) Armaroli, N.; Marconi, G.; Echegoyen, L.; Bourgeois, J. P.; Diederich, F. *Chem. Eur. J.* **2000,** *6,* 1629.
(59) Sandanayaka, A. S. D.; Ikeshita, K.; Watanabe, N.; Araki, Y.; Furusho, Y.; Kihara, N.; Takata, T.; Ito, O. *Bull. Chem. Soc. Jpn.* **2005,** *78,* 1008.
(60) Rehm, D.; Weller, A. *Isr. J. Chem.* **1970,** *8,* 259.
(61) Rehm, D.; Weller, A. *Ber. Bunsen-Ges.* **1969,** *73,* 834.
(62) Fukuzumi, S.; Ohkubo, K.; Imahori, H.; Shao, J. G.; Ou, Z. P.; Zheng, G.; Chen, Y. H.; Pandey, R. K.; Fujitsuka, M.; Ito, O.; Kadish, K. M. *J. Am. Chem. Soc.* **2001,** *123,* 10676.
(63) Imahori, H.; Yamada, H.; Guldi, D. M.; Endo, Y.; Shimomura, A.; Kundu, S.; Yamada, K.; Okada, T.; Sakata, Y.; Fukuzumi, S. *Angew. Chem., Int. Ed.* **2002,** *41,* 2344.
(64) Ito, O. *Res. Chem. Intermed.* **1997,** *23,* 389.
(65) Kato, T.; Kodama, T.; Shida, T.; Nakagawa, T.; Matsui, Y.; Suzuki, S.; Shiromaru, H.; Yamauchi, K.; Achiba, Y. *Chem. Phys. Lett.* **1991,** *180,* 446.
(66) Araki, Y.; Ito, O. *J. Photochem. Photobiol., C* **2008,** *9,* 93.
(67) Sension, R. J.; Phillips, C. M.; Szarka, A. Z.; Romanow, W. J.; Mcghie, A. R.; Mccauley, J. P.; Smith, A. B.; Hochstrasser, R. M. *J. Phys. Chem.* **1991,** *95,* 6075.
(68) Kawauchi, H.; Suzuki, S.; Kozaki, M.; Okada, K.; Islam, D. M. S.; Araki, Y.; Ito, O.; Yamanaka, K. *J. Phys. Chem. A* **2008,** *112,* 5878.
(69) Martin-Gomis, L.; Ohkubo, K.; Fernandez-Lazaro, F.; Fukuzumi, S.; Sastre-Santos, A. *J. Phys. Chem. C* **2008,** *112,* 17694.